

Article

Optimized Device Geometry of Normally-On Field-Plate AlGa_N/Ga_N High Electron Mobility Transistors for High Breakdown Performance Using TCAD Simulation

Sakhone Pharkphoumy¹, Vallivedu Janardhanam¹, Tae-Hoon Jang², Jaejun Park¹, Kyu-Hwan Shim^{1,2,*} and Chel-Jong Choi^{1,*}

¹ School of Semiconductor and Chemical Engineering, Semiconductor Physics Research Center, Chonbuk National University, Jeonju 54896, Korea; psakhone14@gmail.com (S.P.); dr.vjanardhanreddy@gmail.com (V.J.); fpthffl@naver.com (J.P.)

² R&D Center, Sigetronics Inc., Jeonju 55314, Korea; tjang@sigetronics.com

* Correspondence: khshim@jbn.ac.kr (K.-H.S.); cjchoi@jbn.ac.kr (C.-J.C.)

Abstract: This study presents the optimization of the lateral device geometry and thickness of the channel and barrier layers of AlGa_N/Ga_N high electron mobility transistors (HEMTs) for the enhancement of breakdown voltage (V_{BR}) characteristics using a TCAD simulation. The effect of device geometry on the device performance was explored by varying the device design parameters, such as the field plate length (L_{FP}), gate-to-drain length (L_{GD}), gate-to-source length (L_{GS}), gate length (L_G), thickness of the Si₃N₄ passivation layer (T_{ox}), thickness of the Ga_N channel (T_{ch}), and AlGa_N barrier ($T_{barrier}$). The V_{BR} was estimated from the off-state drain current versus the drain voltage ($I_{DS}-V_{DS}$) curve, and it exhibited a strong dependence on the length and thickness of the parameters. The optimum values of V_{BR} for all the device's geometrical parameters were evaluated, based on which, an optimized device geometry of the field-plated AlGa_N/Ga_N HEMT structure was proposed. The optimized AlGa_N/Ga_N HEMT structure exhibited $V_{BR} = 970$ V at $I_{GS} = 0.14$ A/mm, which was considerably higher than the results obtained in previous studies. The results obtained in this study could provide vital information for the selection of the device geometry for the implementation of HEMT structures.

Keywords: AlGa_N/Ga_N; HEMT; device parameters; breakdown voltage; high power; TCAD simulation



check for updates

Citation: Pharkphoumy, S.; Janardhanam, V.; Jang, T.-H.; Park, J.; Shim, K.-H.; Choi, C.-J. Optimized Device Geometry of Normally-On Field-Plate AlGa_N/Ga_N High Electron Mobility Transistors for High Breakdown Performance Using TCAD Simulation. *Electronics* **2021**, *10*, 2642. <https://doi.org/10.3390/electronics10212642>

Academic Editors: Kai Fu and Matteo Meneghini

Received: 16 September 2021

Accepted: 27 October 2021

Published: 28 October 2021

Publisher's Note: MDPI stays neutral with regard to jurisdictional claims in published maps and institutional affiliations.



Copyright: © 2021 by the authors. Licensee MDPI, Basel, Switzerland. This article is an open access article distributed under the terms and conditions of the Creative Commons Attribution (CC BY) license (<https://creativecommons.org/licenses/by/4.0/>).

1. Introduction

AlGa_N/Ga_N high-electron mobility transistors (HEMTs) have attracted extensive attention for high-frequency and high-voltage applications owing to their excellent properties, such as the high electron mobility of their two-dimensional electron gas (2-DEG) channels, their wide energy band-gap, and their high breakdown field [1,2]. It is well known that the breakdown voltage (V_{BR}) of power devices is one of the most important parameters for providing reliable performance for high-power applications; however, the reported values are considerably below the theoretical limit [3–5]. Hence, it is necessary to improve the V_{BR} , especially without increasing the device's size. Trew et al. reported a model that described the dependence of the V_{BR} on the avalanche process associated with the maximum electric field generated at the gate edge toward the drain side, resulting in a drain-to-gate breakdown [6,7].

The high breakdown field of Ga_N allows high voltages to be sustained between the drain and the gate. However, because of the much higher critical electric field of AlGa_N, an early breakdown occurs near the heterointerface [8]. Various edge termination techniques, such as floating gates, field modulating plates, source-extended field plates, and multiple field plates, have been proposed to achieve a high V_{BR} and improve the device performance in AlGa_N/Ga_N HEMTs [9–11]. To enhance the device's performance

for high-voltage power devices and microwave applications, GaN-based HEMTs were developed using field-plate technology, through which tremendous improvements in the V_{BR} and power densities were demonstrated [1,12–16]. The field plate is an extension of the gate deposited onto the passivation layer toward the drain side to minimize the electric field at the AlGaN surface. This leads to a reduction in the DC-to-RF dispersion, resulting in an increase in the V_{BR} [17]. Berzoy et al. [18] demonstrated an improvement in the V_{BR} in an AlGaN/GaN HEMT structure through the inclusion of various field plates on their structures. They reported an optimum V_{BR} of 880 V at a gate current of 40 A/mm for the best field plate case.

In addition to the field plate dimension, the device's geometrical parameters, such as the gate length (L_G), gate width (W), source-drain distance (L_{SD}), source-gate separation (L_{GS}), gate-drain separation (L_{GD}), thicknesses of the Si_3N_4 passivation layer (T_{ox}), GaN channel (T_{ch}), and AlGaN barrier ($T_{barrier}$) can significantly affect the device's characteristics. These parameters are correlated with and affected by each other. In other words, all the geometrical parameters should be tuned to achieve high performance GaN-based HEMTs with field plates. Nevertheless, reports on the effect of the device's geometry on device performance are limited. For instance, as summarized in Table 1, previous reports mainly investigated the effects of a few device geometrical parameters, such as L_{GD} , L_G , and field plate length (L_{FP}), on the operational characteristics of HEMTs, mainly in terms of V_{BR} . Unlike previous simulation studies, which focused primarily on the structural optimization of HEMTs by changing the limited number of geometrical parameters, the present work performed an extensive and systematic investigation of the impact of all the possible device design parameters, such as L_G , W , L_{SD} , L_{GS} , L_{GD} , T_{ox} , T_{ch} , and $T_{barrier}$ on the DC output and V_{BR} characteristics of the field-plated AlGaN/GaN HEMTs, using technology computer aided design (TCAD) simulations. In the present study, the simulation was performed by varying one of the geometrical parameters of the field-plated AlGaN/GaN HEMT structure, while keeping the other geometrical parameters constant. Based on the simulation results, we propose an AlGaN/GaN HEMT structure with optimized device geometry to achieve the best possible device performance in terms of V_{BR} . In addition, a simulation of the output characteristics, transfer curve, and transconductance was performed. The optimized AlGaN/GaN HEMT structure exhibited a V_{BR} of 970 V at $I_{GS} = 0.14$ A/mm. The recorded values of the on-resistance and the power device figure of merit (FOM), defined by V_{BR}^2/R_{ON} [19], were $3.12 \Omega \cdot \text{cm}$ and $0.3 \text{ MV}^2/\Omega \cdot \text{cm}$, respectively. It should be noted that the operational behavior of the devices simulated by varying the key device geometrical parameters, i.e., L_{GD} , L_G , and L_{FP} , showed a similar tendency to previous works. In other words, a thorough comparison of the simulated results demonstrated in this work exhibited a close match with the previously reported experimental and simulated results. This implies that the accuracy, along with the validation, of our simulation approach is sufficient to provide verification of the results, although the present study does not include any experimental verification [20]. Furthermore, the AlGaN/GaN HEMT structure proposed can be achieved from a technological standpoint, of which optimization with realistic means is intricate, expensive, and time consuming. The optimized device design parameters obtained from the simulation in this study provide a potential guideline for the development of high-performance AlGaN/GaN HEMTs.

Table 1. V_{BR} comparison of the various HEMT dimensions of the device structure (S: Simulation, E: Experiment).

Ref. Author, Year	S/E	L_{GD} (μm)	L_G (μm)	L_{FP} (μm)	V_{BR} (V)
[16] Karmalkar. S. (2001)	S	4.7	0.4	2	630
[21] Saito. W. (2003)	E	5	1.5	1.6	350
		10	1.5	5	600
[22] Lin Zhu (2016)	S/E	3	3	-	120
		5	3	-	220
		7	3	-	320
[18] A. Berzoy (2017)	S	6.9	0.7	1.4	880
[23] D. Nirmal (2018)	S	2.7	0.25	1	291
		4	0.25	1	370
		6	0.25	1	420
[24] L. Wang (2018)	S	3	-	-	620
		5	-	-	700
		10	-	-	800
[25] P. Bhavana (2019)	E	4	0.7	-	72
		6	0.7	-	118
[26] A.S.A. Fletcher (2019)	E	2.7	0.25	0.9	300
[5] B. Liao (2019)	S	22	3	4	450
Present Study	S	5	1.5	1.5	970

2. Materials and Methods

The schematic cross-section of the field-plated AlGa_{0.28}GaN/GaN HEMT structure used for the simulation and the corresponding energy band profile is shown in Figure 1. It was obtained using two-dimensional (2D) TCAD device simulator software. The transistor structure consisted of a 2 μm undoped GaN buffer layer on a sapphire substrate, a 200 nm thick GaN channel, and a 15 nm thick Al_{0.28}Ga_{0.72}N barrier layer [27]. The doping concentration of the GaN channel layer and AlGa_{0.28}N barrier layer were assumed to be 10^{15} cm^{-3} and $5 \times 10^{16} \text{ cm}^{-3}$, respectively, which is similar to those reported in Refs. [16,21,23,27]. The Al_{0.25}Ga_{0.75}N barrier layer provides an appropriate confinement of electrons towards the channel from the top. Without intentional doping, a huge number of electrons appears at the GaN channel due to piezoelectric and spontaneous polarization effects, resulting in two-dimensional electron gas (2DEG), as shown in Figure 1b. Si₃N₄ was used as the dielectric because it exhibits a high dielectric constant and good breakdown strength, and helps to avoid the cross-talk and noise interference from the atmosphere [23]. The gate field plate was deposited on the Si₃N₄ passivation layer, and the surface state at the interface between the passivation film and AlGa_{0.28}N was neglected. The source and drain ohmic contacts were formed on the 50 nm thick n-type GaN layer with a doping concentration of $5 \times 10^{19} \text{ cm}^{-3}$ grown on the GaN channel. The simulations were performed using a 2D device simulator and Atlas TCAD device software. The material parameters used in the simulation are listed in Table 2 [16,21,23,27]. The gate electrode formed for the proposed structure was assumed to be metal, with a work function of 5.23 eV. The Newton method was used to solve the built-in equations in the Atlas TCAD, such as the transport equation, and Poisson's equation. The simulations were performed by varying the various device geometrical parameters, such as the L_{FP} , L_{GD} , L_{GS} , L_G , T_{ox} , T_{ch} , and $T_{barrier}$. The V_{BR} was calculated from the off-state drain current versus drain voltage ($I_{DS}-V_{DS}$) curve with a gate bias of $V_G = -6 \text{ V}$. The V_{BR} was determined as the drain voltage for a drain current of 1 mA/mm. Following the simulation results, the values of the geometrical parameters were optimized. These optimized parameter values are included in the caption of Figure 1.

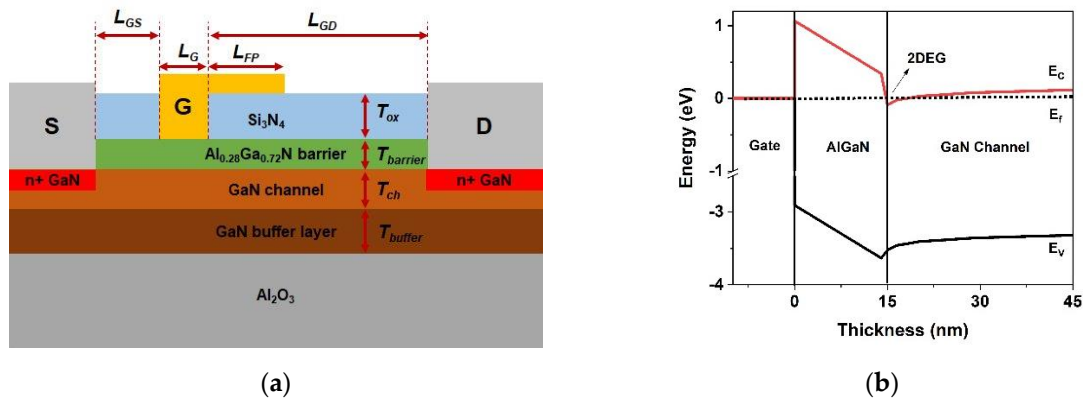


Figure 1. (a) Schematic cross-sectional 2D structure of the AlGaN/GaN HEMT on an insulation substrate with a single-gate field plate (device dimensions of the optimized device structure: $L_{GS} = 2 \mu\text{m}$, $L_{GD} = 5 \mu\text{m}$, $L_G = 1.5 \mu\text{m}$, $L_{FP} = 1.5 \mu\text{m}$, Si_3N_4 passivation layer thickness ($T_{ox} = 200 \text{ nm}$), GaN channel layer thickness ($T_{ch} = 200 \text{ nm}$), GaN buffer layer ($T_{buffer} = 2 \mu\text{m}$), AlGaN barrier layer ($T_{barrier} = 15 \text{ nm}$), and gate width ($W_g = 200 \mu\text{m}$)), and (b) the corresponding energy band profile.

Table 2. Physical parameter of AlGaN/GaN used in Atlas TCAD simulation [16,21,23,27].

TCAD Parameters	GaN	AlGaN	Unit
Electron mobility (μ_n)	900	600	$\text{cm}^2/\text{V}\cdot\text{s}$
Hole mobility (μ_p)	10	10	$\text{cm}^2/\text{V}\cdot\text{s}$
Energy band gap (E_g)	3.40	3.96	eV
Conduction band density of state (N_c)	1.07	2.07	$10^{18}/\text{cm}^3$
Valance band density of state (N_v)	1.16	1.16	$10^{19}/\text{cm}^3$
Saturation velocity (V_{sat})	2.00	1.10	10^7 cm/s
Relative permittivity (ϵ)	9.50	9.50	-
Trap lifetime (e, p)	1	1	10^7 s

3. Results and Discussion

In this study, a TCAD simulation was performed for an AlGaN/GaN HEMT structure, shown in Figure 1, by varying the dimensions of the lateral device geometry. It is well known that the length of the various geometries of the HEMT structure affects the device's performance and V_{BR} . The field plate connected to the gate was introduced to modify the electric field at the gate edge on the drain side, which significantly suppressed the effect of the surface traps and increased the V_{BR} of the HEMT devices [1]. The V_{BR} is directly related to the L_{FP} because the extension of the gate edge point redistributes the peak electric field in the channel layer and reduces the electron punch-through effect. A simulation of the effect of the L_{FP} on the V_{BR} was carried out for the proposed HEMT structure, as shown in Figure 1. The results are depicted in Figure 2 as a function of L_{FP} varying in the range of 0.5–2.5 μm , with the other geometrical parameters constant. It was observed that the V_{BR} increased along with the increase in L_{FP} until it reached a value of 1.5 μm , at a maximum V_{BR} of 956 V. This increase in V_{BR} with an increase in L_{FP} was associated with the formation of a depletion layer under the field plate electrode, which reduces the electric field strength at the gate on the drain side [10]. However, a further increase in the L_{FP} beyond 1.5 μm led to a reduction in the value of the V_{BR} , which was attributed to the increase in the electric field-driven impact ionization process at the drain side of the field plate edge [21,28]. Furthermore, a longer field plate extension increased the main electric field peak under the field plate edge, resulting in an increase in the gate capacitance and a decrease in the V_{BR} [16].

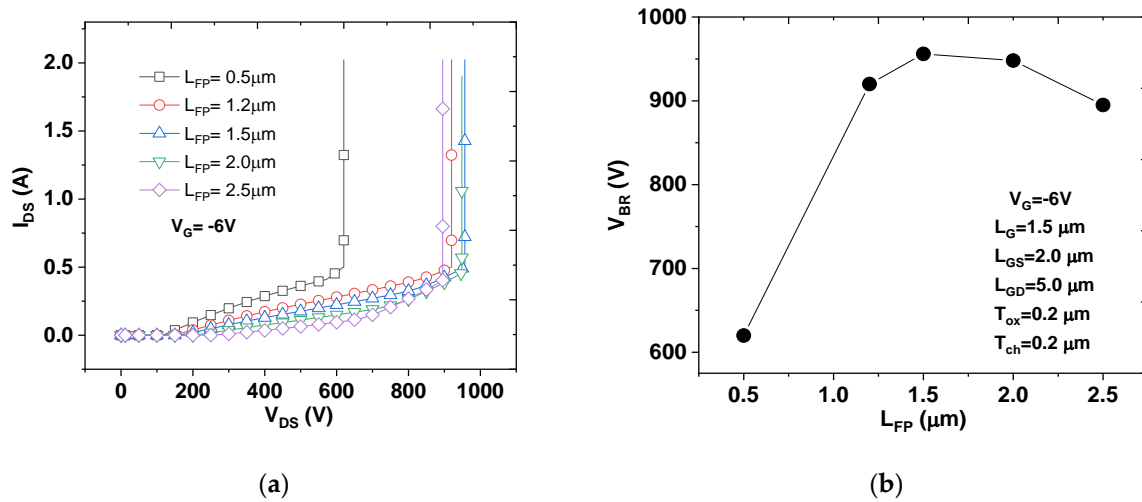


Figure 2. (a) I_{DS} - V_{DS} characteristic curve at bias $V_{GS} = -6\text{ V}$, and (b) V_{BR} at various values of L_{FP} .

It is well known that the L_{GD} affects the V_{BR} characteristics of HEMTs, and an increase in the L_{GD} leads to an increase in the V_{BR} of the device, which is associated with the higher spacing [29]. Figure 3a shows the breakdown characteristics of the AlGaIn/GaN HEMTs at various values of L_{GD} varying in the range of 3–15 μm . Figure 3b shows the variation in the V_{BR} with respect to the L_{GD} . It is evident that the V_{BR} increased along with the increase in the L_{GD} . This may have been associated with the reduction in the peak electric field at the gate edge of the drain side. However, V_{BR} strongly depends on the electric field at the gate field-plate edge on the drain side. Further, it can be observed from Figure 3a that the breakdown occurred at $I_{DS} = 0.5\text{ A}$, regardless of the L_{GD} . Figure 3 shows the V_{BR} characteristics for the field-plated AlGaIn/GaN HEMT, with the device's structure shown in Figure 1a, as a function of varying gate-drain lengths in the range of 3–15 μm at $V_{GS} = -6\text{ V}$. It is noteworthy that the drain current remained constant until a voltage of 400 V, regardless of the L_G . However, for $L_{GD} = 3\ \mu\text{m}$, the current increased drastically for voltages greater than 400 V. For the AlGaIn/GaN HEMT, the current levels were sustained until higher voltages, which increased with an increase in the L_{GD} . From Figure 3b, it can be observed that the V_{BR} increased to 600 V, 900 V, 1150 V, and 1175 V, with an increase in the L_{GD} of 3 μm , 5 μm , 10 μm , and 15 μm . The V_{BR} increased proportionally with the increase in the L_{GD} when the breakdown was primarily due to the high electric field at the drain side of the gate edge. As the L_{GD} increased, the electric field at the gate edge reduced, with an increase in the distance between the gate and the drain. The breakdown voltage increased along with the increase in the L_{GD} associated with the increased parasitic channel resistance [30].

Figure 4 displays the V_{BR} curves of the AlGaIn/GaN HEMT at various values of L_{GS} varying from 1 μm to 5 μm . Figure 4b depicts the values of V_{BR} with the variation in L_{GS} at $V_G = -6\text{ V}$. It is notable that the impact of the L_{GS} on the I_{DS} was negligible. The V_{BR} increased along with the increase in the L_{GS} at $V_G = -6\text{ V}$, resulting in the extraction of higher output power. Unlike an increase in L_{GD} , an increase in L_{GS} does not increase the width of the leakage path. This is because at high leakage, the current flows primarily through the source terminal, and not the source-side channel. Therefore, an increase in the L_{GS} will lead to an increase in the resistance of the bugger layer, resulting in an increase in the V_{BR} . This could be associated with the increase in the space between the source and gate, enabling the distribution of the electric field over a wider area. As shown in Figure 4, the L_{GS} increased as a function of V_{BR} . As shown in the plot of the simulation results, the V_{BR} increased along with the increases in the L_{GS} of 1 μm , 2 μm , 3 μm , and 5 μm at $V_G = -6\text{ V}$, which then increased to 885 V, 920 V, 930 V, and 980 V, respectively. The enhancement in the electric field with the spacer between the source and the gate resulted in the improvement of the V_{BR} performance. The optimization of L_{GS} has a significant

impact on the V_{BR} of the device. This is because of the source-injection buffer leakage, in contrast to the decrease in V_{BR} caused by the increase in L_{GD} , with the decrease in the width of the current flow.

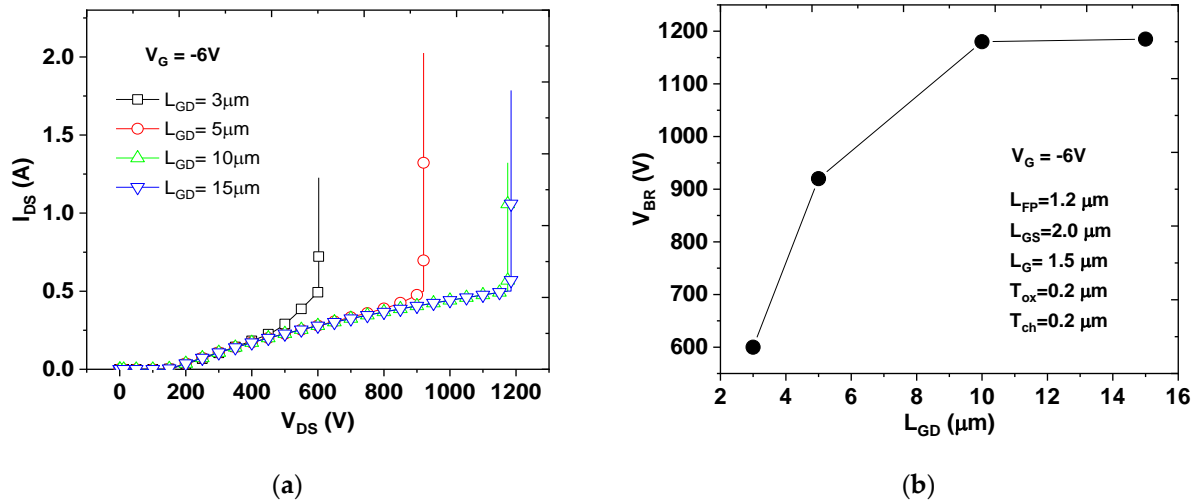


Figure 3. (a) I_{DS} - V_{DS} characteristic curve at bias $V_{GS} = -6 V$, and (b) V_{BR} at various values of L_{GD} .

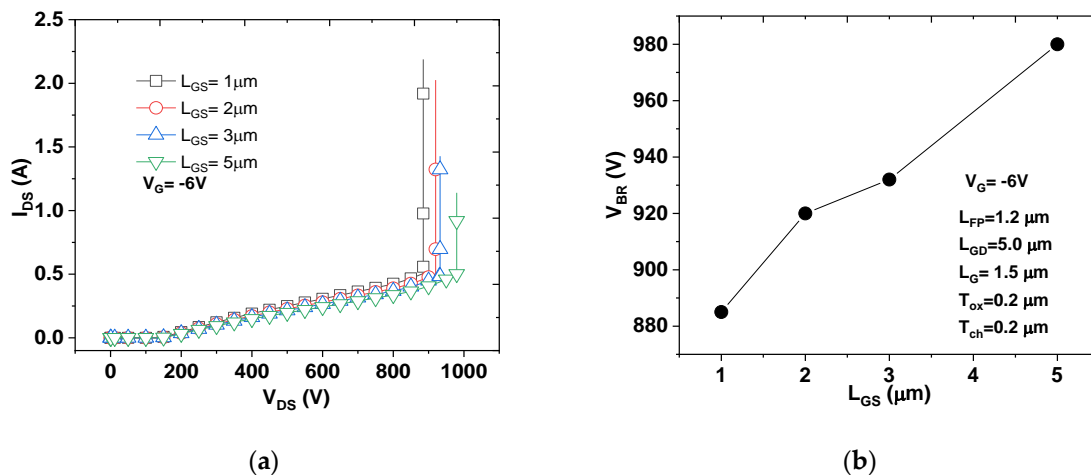


Figure 4. (a) I_{DS} - V_{DS} characteristic curve at bias $V_{GS} = -6 V$, and (b) V_{BR} at various values of L_{GS} .

Figure 5a shows the V_{BR} characteristics of the AlGaIn/GaN HEMTs as a function of L_G varying from $0.2\mu m$ to $2.5\mu m$. As the L_G increased, the area of the gate electrode increased, while the areas of the source and drain electrodes remained the same. The leakage current decreased along with an increase in L_G . As can be observed in Figure 5b, the V_{BR} increased along with the increase in L_G , varying in the range of 110–960 V, with the L_G varying in the range of 0.2 – $2.5\mu m$. Furthermore, the current levels were lowered significantly with the increase in L_G . This could be due to the fact that an increase in L_G suppresses the punch-through and improves V_{BR} [31]. In addition, a higher value of L_G lowers the impact ionization at the gate edge on the drain side, which significantly lowers the leakage current. Additionally, a higher value of L_G effectively suppresses the drain-induced barrier lowering [32].

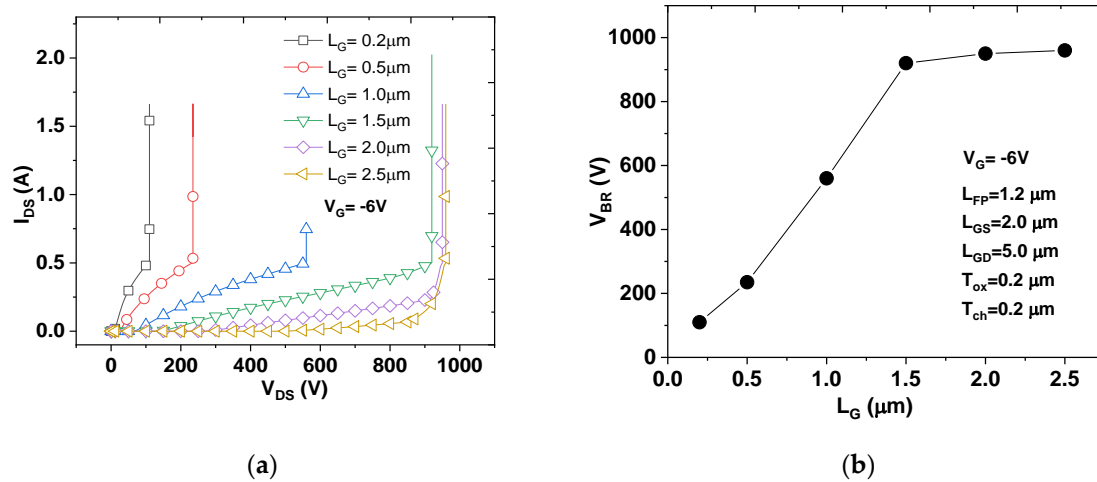


Figure 5. (a) I_{DS} - V_{DS} characteristic curve at bias $V_{GS} = -6\text{ V}$, and (b) V_{BR} at various values of L_G .

The V_{BR} behavior of the AlGaIn/GaN heterostructure field-plated HEMT as a function of the thickness of the Si_3N_4 insulator passivation layer was investigated through simulation. Figure 6a shows the variation in the V_{BR} of the AlGaIn/GaN HEMTs as a function of the Si_3N_4 thickness in the range of 0.1–0.7 μm . It is noteworthy that the leakage current increased along with the increase in Si_3N_4 thickness. By contrast, it can be observed from Figure 6b that the V_{BR} of the HEMT increased initially, exhibiting a higher value of 970 V for the Si_3N_4 layer with a thickness of 0.2 μm , followed by a drastic decrease in the V_{BR} along with increasing thickness of the Si_3N_4 insulator passivation layer. Generally, in the case of an insulator layer with thickness at the lower end of a certain thickness range, the electric field is concentrated at the field plate edge. Conversely, for a layer with maximum thickness, the field concentration is at the gate edge [17]. For a layer with an optimum thickness, the field is distributed between the gate edge and the field plate edge. The observed decrease in the V_{BR} with an increase in the thickness above 0.2 μm (the optimum thickness) implies that the nitride layer used was extremely thick and the field plate was far away from the semiconductor, so that the field plate did not have any effect on the electric field distribution. This demands the optimization of the thickness of the insulator passivation layer to produce a high-performance AlGaIn/GaN HEMT.

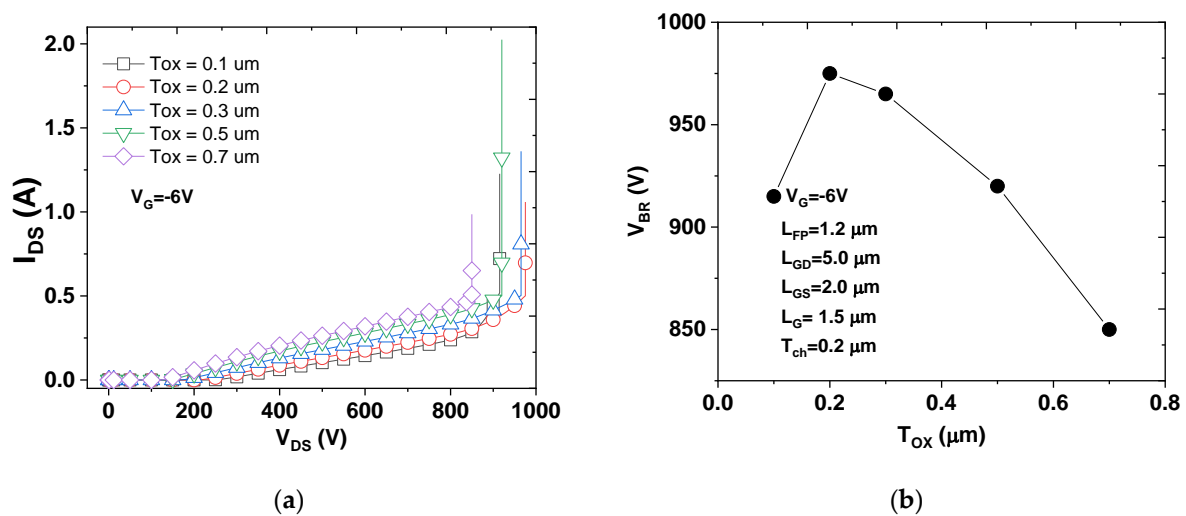


Figure 6. (a) I_{DS} - V_{DS} characteristic curve at bias $V_{GS} = -6\text{ V}$, and (b) V_{BR} at various values of thickness of the Si_3N_4 under the field plate (T_{ox}).

Figure 7a shows the V_{BR} characteristics of the AlGaIn/GaN HEMT as a function of the GaN channel layer thickness (T_{ch}) varying between 100 nm, 200 nm, 500 nm, 1000 nm, and 2000 nm. From Figure 7a, it can be seen that the leakage current increased along with the increase in the channel layer thickness. This resulted in a decrease in the V_{BR} , as shown in Figure 7b. This increase in leakage current with an increase in the channel layer thickness was associated with the wider current path and higher 2DEG concentration resulting from the thicker channel region. This lowered the channel resistance, which tends to lower the V_{BR} . Furthermore, the decrease in V_{BR} might have been associated with the increase in the drain-induced barrier lowering with an increase in the channel thickness. In addition, the deterioration of the gate control causes higher punch-through leakage [33].

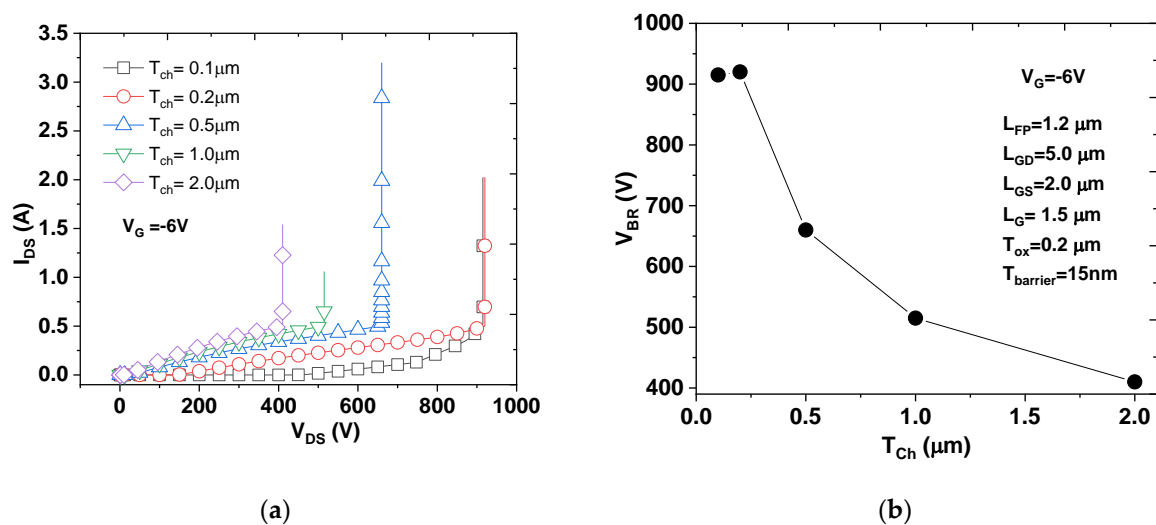


Figure 7. (a) I_{DS} – V_{DS} characteristic curve at bias $V_{GS} = -6V$, and (b) V_{BR} at various values of thickness of the GaN channel (T_{ch}).

Figure 8a shows the V_{BR} characteristic curves of the AlGaIn/GaN HEMTs as a function of the AlGaIn barrier layer thickness varying in the range of 10–35 nm. It was observed that the drain current increased slightly along with the increase in the thickness of the AlGaIn barrier layer. A total of $V_{BR} = 860V$ was obtained for the AlGaIn/GaN HEMT (Figure 8b) with an AlGaIn barrier layer thickness of 10 nm. The V_{BR} increased to 935 V along with the increase in the thickness of the AlGaIn barrier layer to 15 nm, and subsequently decreased along with the increase in the thickness of the AlGaIn barrier layer. This implies that the critical value of the thickness of the AlGaIn barrier layer is 15 nm for effective device operation. The decrease in the V_{BR} below a certain critical value of the thickness of the AlGaIn barrier layer could be explained as follows. For the AlGaIn/GaN HEMT with low AlGaIn barrier thickness, the surface donor-like trap level was below the Fermi level. At the critical barrier thickness, the surface traps reached the Fermi level and the electrons from these traps were driven into the channel by the strong polarization-induced electric field in AlGaIn, creating the 2DEG and leaving behind the positive charge [34]. Until all the surface traps were empty, the Fermi level remained essentially at the donor energy and an increase in the number of electrons transferred with an increase in the barrier thickness. As the negative voltage was increased, the electrons from the gate might have leaked into the trap states in the ungated surfaces and created a “virtual gate” modulating the depletion region. This abrupt change in the gate voltage led to the RF drain current collapse phenomenon.

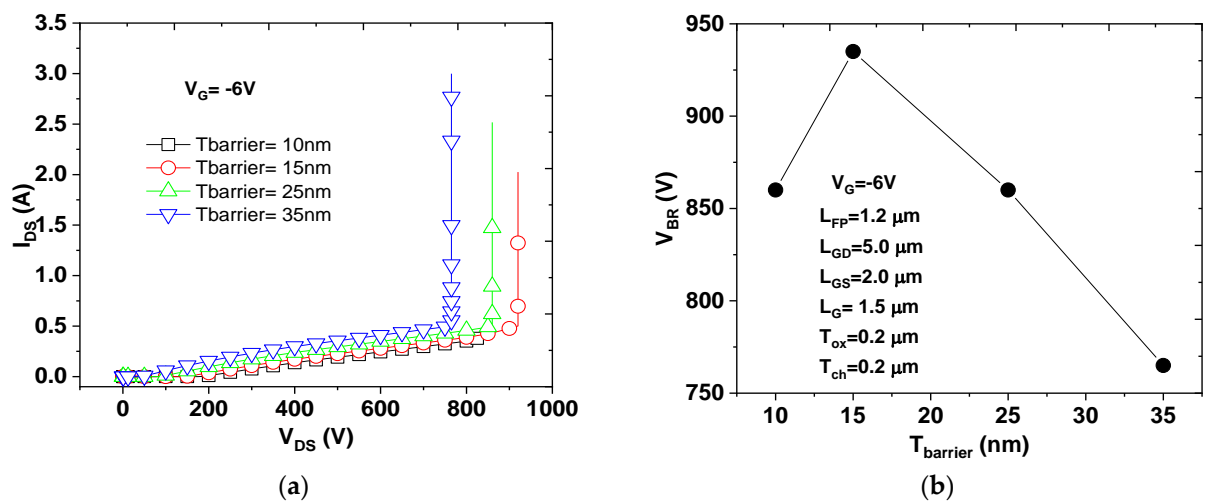


Figure 8. (a) I_{DS} - V_{DS} characteristic curve at bias $V_{GS} = -6\text{ V}$, and (b) V_{BR} at various values of thickness of the AlGaN barrier ($T_{barrier}$).

The simulated output and transfer characteristics of the proposed field-plated AlGaN/GaN HEMT structure shown in Figure 1, with an optimized geometry of $L_{GS} = 2\ \mu\text{m}$, $L_G = 1.5\ \mu\text{m}$, $L_{GD} = 5\ \mu\text{m}$, $T_{ox} = 0.2\ \mu\text{m}$, and $L_{FP} = 1.5\ \mu\text{m}$, are presented in Figure 9a,b, respectively. The I_{DS} - V_{DS} characteristics in Figure 9a are shown as a function of V_{GS} varying from -4 V to $+1\text{ V}$ in steps of 1 V . It can be noted that the current increased distinctly along with the increase in V_{GS} . The drain current I_{DS} was 186 mA/mm at 14 V for $V_{GS} = 0\text{ V}$. Figure 9b displays the corresponding transfer characteristic and transconductance curve at $V_{DS} = 10\text{ V}$. The device exhibited a V_{th} of approximately -4 V , I_{max} of 310 mA/mm at $V_{GS} = 2\text{ V}$, and a peak transconductance (G_m) of 70 mS/mm at $V_{GS} = 1\text{ V}$. The V_{BR} of the optimized device structure with the gate bias was maintained at -6 V , and the device displayed a value of 970 V at $I_{GS} = 0.14\text{ A/mm}$, as shown in Figure 9c. The various values obtained from the optimized AlGaN/GaN HEMT structure are mentioned in Figure 1 and the results are presented in Table 2. An on-resistance (R_{ON}) of $3.12\ \Omega\text{ cm}$, determined by the slope of the I_{DS} - V_{DS} curve at $V_{GS} = 0\text{ V}$, and the power device figure of merit (FOM) of $0.3\text{ MV}^2/\Omega\text{ cm}$, are comparable with the results obtained from the simulated and experimentally fabricated devices possessing various HEMT structures reported earlier.

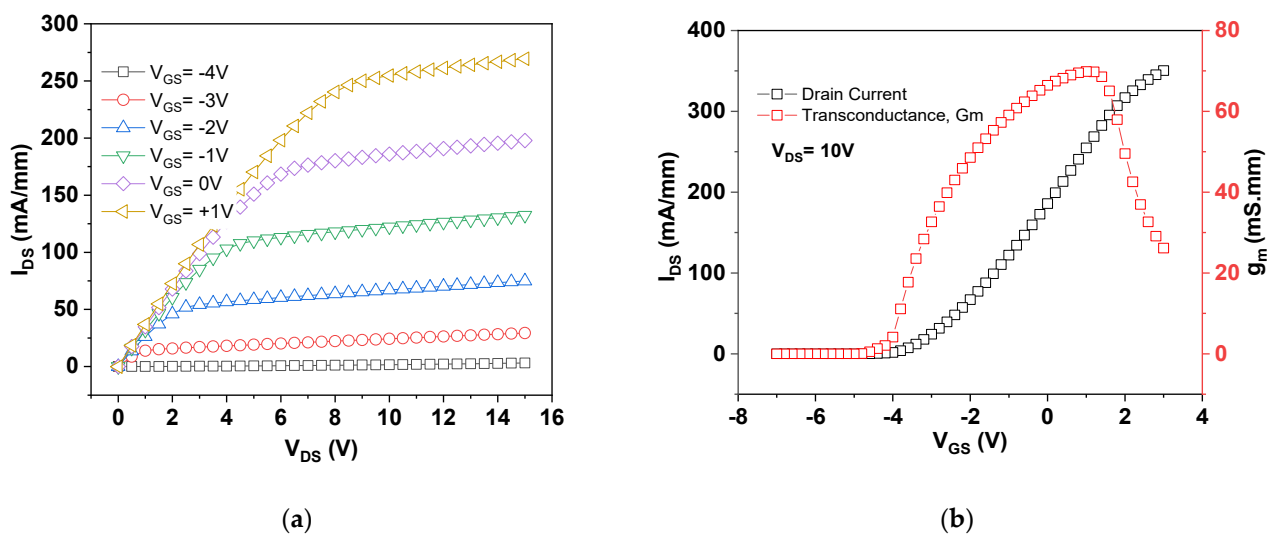


Figure 9. Cont.

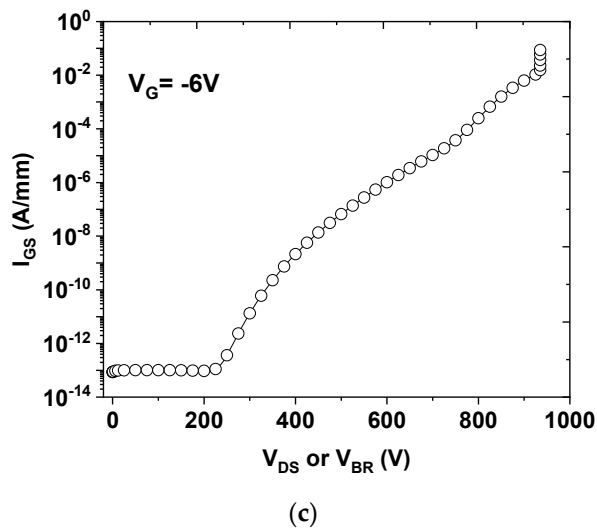


Figure 9. Optimized AlGaIn/GaN HEMT structure (a) I_{DS} – V_{DS} characteristic curve at bias $V_{DS} = 10$ V, (b) I_{DS} and g_m versus V_{GS} characteristic curve, and (c) I_{GS} versus V_{BR} or V_{DS} characteristic curve.

4. Conclusions

The impact of device geometry and the thickness of the channel and barrier layer on the V_{BR} characteristics of field-plated AlGaIn/GaN high-electron mobility transistors (HEMTs) was explored using Atlas TCAD numerical simulation. The effect of device geometry was investigated by varying the parameters, such as the L_{FP} , L_{GD} , L_{GS} , L_G , T_{ox} , T_{ch} , and $T_{barrier}$. The V_{BR} strongly depends on the length and thickness of the aforementioned parameters. Based on the optimum V_{BR} values obtained for all the geometrical parameters, an optimized device geometry of the field-plated AlGaIn/GaN HEMT structure was proposed following a simulation of the output, transfer characteristics, and transconductance. A V_{BR} of 970 V was obtained at $I_{GS} = 0.14$ A/mm for the optimized AlGaIn/GaN HEMT structure. This optimized device geometry of the proposed AlGaIn/GaN HEMT structure could be useful for the implementation of HEMT-structured AlGaIn/GaN heterostructures.

Author Contributions: Conceptualization, S.P. and V.J.; methodology, S.P.; formal analysis, S.P., V.J., T.-H.J. and J.P.; writing—original draft preparation, S.P.; writing—review and editing, K.-H.S. and C.-J.C.; supervision, K.-H.S. and C.-J.C. All authors have read and agreed to the published version of the manuscript.

Funding: This study was supported by the Korea Evaluation Institute of Industrial Technology (KEIT) grant (Project No. 20004314), funded by the Ministry of Trade, Industry and Energy, Republic of Korea, and by the Korea Electric Power Corporation (Grant number: R20XO01-10).

Conflicts of Interest: The authors declare no conflict of interest. The funding agencies had no role in the decision to publish the results.

References

1. Cho, K.-H.; Kim, Y.-S.; Lim, J.; Choi, Y.-H.; Han, M.-K. Design of AlGaIn/GaN HEMTs employing mesa field plate for breakdown voltage enhancement. *Solid State Electron.* **2010**, *54*, 405–409. [[CrossRef](#)]
2. Wang, X.; Huang, S.; Zheng, Y.; Wei, K.; Chen, X.; Zhang, H.; Liu, X. Effect of GaN channel layer thickness on DC and RF performance of GaN HEMTs with composite AlGaIn/GaN buffer. *IEEE Trans. Electron Devices* **2014**, *61*, 1341–1346. [[CrossRef](#)]
3. Lee, Y.; Yao, Y.; Huang, C.; Lin, T.; Cheng, L.; Liu, C.; Wang, M.; Hwang, J. High breakdown voltage in AlGaIn/GaN HEMTs using AlGaIn/GaN/AlGaIn quantum-well electron-blocking layers. *Nanoscale Res. Lett.* **2014**, *9*, 433. [[CrossRef](#)] [[PubMed](#)]
4. Dora, Y.; Chakraborty, A.; McCarthy, L.; Keller, S.; DenBaars, S.P.; Mishra, U.K. High Breakdown Voltage Achieved on Al-GaN/GaN HEMTs With Integrated Slant Field Plates. *IEEE Electron Device Lett.* **2006**, *27*, 713–715. [[CrossRef](#)]
5. Liao, B.; Zhou, Q.; Qin, J.; Wang, H. Simulation of AlGaIn/GaN HEMTs' breakdown voltage enhancement using gate field-plate, source field-plate and drain field plate. *Electronics* **2019**, *8*, 406. [[CrossRef](#)]
6. Zhang, N.Q.; Keller, S.; Parish, G.; Heikman, S.; BenBaars, S.P.; Mishra, U.K. High breakdown in GaN HEMT with overlapping gate structure. *IEEE Electron Device Lett.* **2000**, *21*, 421–423. [[CrossRef](#)]

7. Trew, R.J.; Mishra, U.K. Gate breakdown in MESFET's and HEMT's. *IEEE Electron Device Lett.* **1991**, *12*, 524–526. [[CrossRef](#)]
8. Zhang, P.; Zhao, S.-L.; Hou, B.; Wang, C.; Zheng, X.-F.; Ma, X.-H.; Zhang, J.-C.; Hao, Y. Improvement of the off-state breakdown voltage with field plate and low-density drain in AlGaN/GaN high-electron mobility transistors. *Chin. Phys. B* **2015**, *24*, 037304. [[CrossRef](#)]
9. Wu, Y.F.; Moore, M.; Wisleder, T.; Chavarkar, P.M.; Mishra, U.K.; Parikh, P. High Gain Microwave GaN HEMTs with Source-Terminated Field-Plates. In Proceedings of the IEDM Technical Digest. IEEE International Electron Devices Meeting, San Francisco, CA, USA, 13–15 December 2004. [[CrossRef](#)]
10. Ando, Y.; Okamoto, Y.; Miyamoto, H.; Nakayama, T.; Inoue, T.; Kuzuhara, M. 10-W/mm AlGaN-GaN HFET with a field modulating plate. *IEEE Electron Device Lett.* **2003**, *24*, 289–291. [[CrossRef](#)]
11. Ando, Y.; Wakejima, A.; Okamoto, Y.; Nakayama, T.; Ota, K.; Yamanoguchi, K.; Murase, Y.; Kasahara, K.; Matsunaga, K.; Inoue, T.; et al. Novel AlGaN/GaN Dual-field-plate FET with high gain, increased linearity and stability. In Proceedings of the IEEE International Electron Devices Meeting, Washington, DC, USA, 5 December 2005. [[CrossRef](#)]
12. Lee, J.G.; Lee, H.J.; Cha, H.Y. Field plated AlGaN/GaN-on-Si HEMTs for high voltage switching applications. *J. Korean Phys. Soc.* **2011**, *59*, 2297–2300. [[CrossRef](#)]
13. Kumar, V.; Chen, G.; Guo, S.; Adesida, I. Field-plated 0.25- μm gate-length AlGaN/GaN HEMTs with varying field-plate length. *IEEE Trans. Electron Devices* **2006**, *53*, 1477–1480. [[CrossRef](#)]
14. Remashan, K.; Huang, W.P.; Chyi, J.I. Simulation and fabrication of high voltage AlGaN/GaN based Schottky diodes with field plate edge termination. *Microelectron. Eng.* **2007**, *84*, 2907–2915. [[CrossRef](#)]
15. Kaddeche, M.; Telia, A.; Soltani, A. Analytical modeling and analysis of Al m Ga1-m N/GaN HEMTs employing both field-plate and high-k dielectric stack for high-voltage operation. *J. Comput. Electron.* **2013**, *12*, 501–510. [[CrossRef](#)]
16. Karmalkar, S.; Mishra, U. Enhancement of breakdown voltage in AlGaN/GaN high electron mobility transistors using a field plate. *IEEE Trans. Electron Devices* **2001**, *48*, 1515–1521. [[CrossRef](#)]
17. Karmalkar, S.; Shur, M.S.; Simin, G.; Asif Khan, M. Field-plate engineering for HFETs. *IEEE Trans. Electron Devices* **2005**, *52*, 2534–2540. [[CrossRef](#)]
18. Berzoy, C.; Lashway, R.; Moradisizkoohi, H.; Mohammed, O.A. Breakdown voltage improvement and analysis of GaN HEMTs through field plate inclusion and substrate removal. In Proceedings of the 2017 IEEE 5th Workshop on Wide Bandgap Power Devices and Applications (WiPDA), Albuquerque, NM, USA, 30 October–1 November 2017. [[CrossRef](#)]
19. Anand, M.J.; Ng, G.I.; Arulkumaran, S.; Wang, H.; Li, Y.; Vicknesh, S.; Egawa, T. Low Specific ON-resistance and High Figure-of-Merit AlGaN/GaN HEMTs on Si substrate with Non-Gold Metal Stacks. In Proceedings of the 71st Device Research Conference, Notre Dame, IN, USA, 23–26 June 2013. [[CrossRef](#)]
20. Ghione, G. Looking for Quality in TCAD-Based Papers. *IEEE Trans. Electron Device* **2019**, *8*, 3252–3253. [[CrossRef](#)]
21. Saito, W.; Kuraguchi, M.; Takada, Y.; Tsuda, K.; Omura, I.; Ogura, T. Design Optimization of High Breakdown Voltage AlGaN-GaN Power HEMT on an Insulating Substrate for RONA-VB Tradeoff Characteristics. *IEEE Trans. Electron Device* **2005**, *52*. [[CrossRef](#)]
22. Zhu, L.; Wang, J.; Jiang, H.; Wang, H.; Wu, W.; Zhou, Y.; Dai, G. Theoretical Analysis of Buffer Trapping Effects on off-State Breakdown between Gate and Drain in AlGaN/GaN HEMTs. In Proceedings of the 2016 International Conference on Integrated Circuits and Microsystems (ICICM), Chengdu, China, 23–25 November 2016. [[CrossRef](#)]
23. Nirmal, D.; Arivazhagan, L.; Fletcher, A.A.S.; Ajayan, J.; Prajoun, P. Current collapse modeling in AlGaN/GaN HEMT using small signal equivalent circuit for high power application. *Superlattices Microstruct.* **2018**, *113*, 810–820. [[CrossRef](#)]
24. Wang, L.; Wang, S.; Tan, C.; Ye, H.; Luo, H.; Chen, X. The Breakdown Voltage of AlGaN/GaN HEMT is Restricted to The Structure Parameters of The Device: A Study Based on TCAD. In Proceedings of the 2018 19th International Conference on Electronic Packaging Technology (ICEPT), Shanghai, China, 8–11 August 2018. [[CrossRef](#)]
25. Bhavana, P.; Mishra, S.; Karmalkar, S. Analysis of the Significant Rise in Breakdown Voltage of GaN HEMTs from Near-Threshold to Deep Off-State Gate Bias Conditions. *IEEE Trans. Device Mater. Reliability* **2019**, *19*, 766–773. [[CrossRef](#)]
26. Fletcher, A.A.S.; Nirmal, D.; Ajayan, J.; Arivazhagan, L. Analysis of AlGaN/GaN HEMT using discrete field plate technique for high power and high frequency applications. *Int. J. Electron. Commun.* **2019**, *99*, 325–330. [[CrossRef](#)]
27. Jebalin, B.K.; Rekh, S.A.; Prajoun, P.; Kumar, M.N.; Nirmal, D. The influence of high-k passivation layer on breakdown voltage of Schottky AlGaN/GaN HEMTs. *Microelectron. J.* **2015**, *46*, 1387–1391. [[CrossRef](#)]
28. Kabemura, T.; Ueda, S.; Kawada, Y.; Horio, K. Enhancement of Breakdown Voltage in AlGaN/GaN HEMTs: Field plate Plus High-k Passivation layer and High Acceptor density in Buffer Layer. *IEEE Trans. Electron Devices* **2018**, *65*, 3848–3854. [[CrossRef](#)]
29. Neha, N.; Kumari, V.; Gupta, M.; Saxena, M. Simulation based breakdown voltage analysis of 3-step field plate AlGaN/GaN HEMT. In Proceedings of the 2018 4th International Conference on Devices, Circuits and Systems (ICDCS), Coimbatore, India, 16–17 March 2018. [[CrossRef](#)]
30. Baliga, B.J. Trends in power semiconductor devices. *IEEE Trans. Electron. Devices* **1996**, *43*, 1717–1731. [[CrossRef](#)]
31. Uren, M.; Nash, K.; Balmer, R.; Martin, T.; Morvan, E.; Caillas, N.; Delage, S.; Ducatteau, D.; Grimbert, B.; De Jaeger, J. Punch-through in short-channel AlGaN/GaN HFETs. *IEEE Trans. Electron. Devices* **2006**, *53*, 395–398. [[CrossRef](#)]
32. Luo, J.; Zhao, S.-L.; Mi, M.-H.; Chen, W.-W.; Hou, B.; Zhang, J.-C.; Ma, X.-H.; Hao, Y. Effect of gate length on breakdown voltage in AlGaN/GaN high-electron-mobility transistor. *Chin. Phys. B* **2016**, *25*, 027303. [[CrossRef](#)]

-
33. Xiao-Hua, M.; Ya-man, Z.; Xin-Hua, W.; Ting-Ting, Y.; Lei, P.; Wei-Wei, C.; Xin-Yu, L. Breakdown mechanisms in AlGa_N/Ga_N high electron mobility transistors with different Ga_N channel thickness values. *Chin. Phys. B* **2015**, *24*, 027101. [[CrossRef](#)]
 34. Ibbetson, J.P.; Fini, P.T.; Ness, K.D.; DenBaars, S.P.; Speck, J.S.; Mishra, U.K. Polarization effects, surface states, and the source of electrons in AlGa_N/Ga_N heterostructure field effect transistors. *Appl. Phys. Lett.* **2000**, *77*, 250–252. [[CrossRef](#)]